Electromagnetic form factors of octet baryons with the nonlocal chiral effective theory

Mingyang Yang[1,2] and P. Wang[1,3]

[1]*Institute of High Energy Physics, CAS, P.O. Box 918(4), Beijing 100049, China*
[2]*School of Physical Sciences, University of Chinese Academy of Sciences, Beijing 101408, China*
[3]*Theoretical Physics Center for Science Facilities, CAS, Beijing 100049, China*

The electromagnetic form factors of octet baryons are investigated with the nonlocal chiral effective theory. The nonlocal interaction generates both the regulator, which makes the loop integral convergent, and the Q^2 dependence of form factors at tree level. Both octet and decuplet intermediate states are included in the one-loop calculation. The momentum dependence of baryon form factors is studied up to 1 GeV^2 with the same number of parameters as for the nucleon form factors. The obtained magnetic moments of all the octet baryons as well as the radii are in good agreement with the experimental data and/or lattice simulation.

I. INTRODUCTION

The study of electromagnetic form factors of hadrons is of crucial importance to understand their substructure. A lot of theoretical and experimental efforts have been made in this field. On the one hand, with the upgrade of experimental facilities, the parton distribution functions (PDFs) from the deep inelastic scattering as well as the form factors at relatively large momentum transfer from the elastic scattering can be extracted [1,2]. On the other hand, many measurements on form factors have been carried out at very small momentum transfer to get the information of the nucleon radii as accurate as possible [3,4].

Theoretically, though QCD is the fundamental theory to describe strong interactions, it is difficult to study hadron physics using QCD directly. There are many phenomenological models, such as the cloudy bag model [5], the constituent quark model [6], the 1/Nc expansion approach [7], the Nambu-Jona-Lasino (NJL) model [8], the perturbative chiral quark model (PCQM) [9], the extended vector meson dominance model [10], the SU(3) chiral quark model [11], the quark-diquark model [12], and so on. These model calculations are helpful to provide the physical scenario for the hadron structure.

Besides the phenomenological quark models, there are two systematic methods in hadron physics. One is the lattice simulation and the other is an effective field theory (EFT) of QCD, chiral perturbation theory (ChPT).

Historically, most formulations of ChPT are based on dimensional or infrared regularization (IR). Alhough ChPT is a successful approach, for the nucleon electromagnetic form factors, it is only valid for $Q^2 < 0.1$ GeV^2 [13]. When vector mesons are included, the result is close to the experiments when Q^2 is less than 0.4 GeV^2 [14]. An alternative regularization method, namely finite-range regularization (FRR) has been proposed. Inspired by quark models that account for the finite-size of the nucleon as the source of the pion cloud, effective field theory with FRR has been widely applied to extrapolate lattice data of vector meson mass, magnetic moments, magnetic form factors, strange form factors, charge radii, first moments of GPDs, nucleon spin, etc., [15–24].

Recently, we proposed a nonlocal chiral effective Lagrangian which makes it possible to study the hadron properties at relatively large Q^2 [25,26]. The nonlocal interaction generates both the regulator which makes the loop integral convergent and the Q^2 dependence of form factors at tree level. The obtained electromagnetic form factors and strange form factors of the nucleon are very close to the experimental data [25,26]. This nonlocal chiral effective theory was also applied to study the parton distribution functions and Sivers functions of the sea quarks in nucleons [27,28]. In addition, the nonlocal behavior is further assumed to be a general property for all the interactions and an example of this assumption is the application to the lepton anomalous magnetic moments [29].

Since the nonlocal effective theory provides good descriptions of the nucleon form factors up to relatively large momentum transfer, in this paper, we will extend our study from nucleon to all the octet baryons. While the nucleon form factors are precisely determined experimentally, those

of the other octet baryons are significantly more challenging to measure and as a result are poorly known from nature. Compared with the experiments, for the lattice gauge theory, it is not very difficult to extend the simulation of the nucleon form factors to the other octet form factors. Some lattice simulations on octet form factors have been reported [30–32].

The form factors of octet baryons were also studied in heavy baryon and relativistic chiral perturbation theory with different regularization schemes. In Ref. [33], the magnetic moments and electromagnetic radii of octet baryons were calculated in relativistic ChPT with infrared regularization. The electromagnetic form factors up to $0.4~\text{GeV}^2$ were further studied with the inclusion of vector mesons. The magnetic moments of octet baryons were also studied in relativistic ChPT with an extendend-on-mass-shell (EOMS) renormalization scheme, where the intermediate decuplet states were not included [34]. In

Refs. [35,36], the decuplet states were included in the calculation of octet-baryon form factors with the EOMS scheme. In particular, vector mesons were included explicitly to improve the final results in Ref. [36].

Here, we will apply the nonlocal chiral effective theory to investigate the electromagnetic form factors of all the octet baryons up to $1~\text{GeV}^2$ as well as the magnetic moments and radii. The paper is organized as follows. In Sec. II, we will introduce the nonlocal chiral Lagrangian and the expressions for the form factors are written in the Appendix. Numerical results are presented in Sec. III and finally, Sec. IV gives a short summary.

II. FORMALISM

The lowest order chiral Lagrangian for baryons, pseudoscalar mesons and their interactions can be written as [25,27,37,38]

$$
\mathcal{L} = i\text{Tr}(\bar{B}\gamma_\mu \mathcal{D}^\mu B) - m_B\text{Tr}(\bar{B}B) + \bar{T}^{abc}_\mu(i\gamma^{\mu\nu\alpha}D_\alpha - m_T\gamma^{\mu\nu})T^{abc}_\nu + \frac{f^2}{4}\text{Tr}(\partial_\mu U\partial^\mu U^\dagger)
$$

$$
+ D\text{Tr}(\bar{B}\gamma_\mu\gamma_5\{A^\mu, B\}) + F\text{Tr}(\bar{B}\gamma_\mu\gamma_5[A^\mu, B]) + \frac{\mathcal{C}}{f}\epsilon^{abc}\bar{T}_{\mu,a}{}^{de}(g^{\mu\nu} + z\gamma^\mu\gamma^\nu)B_{ce}\partial_\nu\phi_{bd} + H.C, \tag{1}
$$

where D, F, and $\mathcal{C}$ are the coupling constants. z is the off-shell parameter. The chiral covariant derivative $\mathcal{D}_\mu$ is defined as $\mathcal{D}_\mu B = \partial_\mu B + [V_\mu, B]$. The pseudoscalar meson octet couples to the baryon field via the vector and axial-vector combinations as

$$
V_\mu = \frac{1}{2}(\zeta\partial_\mu\zeta^\dagger + \zeta^\dagger\partial_\mu\zeta) + \frac{1}{2}ie\mathcal{A}_\mu(\zeta^\dagger Q_c\zeta + \zeta Q_c\zeta^\dagger),
$$

$$
A_\mu = \frac{i}{2}(\zeta\partial_\mu\zeta^\dagger - \zeta^\dagger\partial_\mu\zeta) - \frac{1}{2}e\mathcal{A}_\mu(\zeta Q_c\zeta^\dagger - \zeta^\dagger Q_c\zeta), \tag{2}
$$

where

$$
\zeta^2 = U = e^{i2\phi/f}, \qquad f = 93~\text{MeV}. \tag{3}
$$

Q_c is the real charge matrix $\text{diag}(2/3, -1/3, -1/3)$. ϕ and B are the matrices of pseudoscalar fields and octet baryons. $\mathcal{A}_\mu$ is the photon field. The covariant derivative D_μ in the decuplet sector is defined as $D_\nu T^{abc}_\mu = \partial_\nu T^{abc}_\mu + (\Gamma_\nu, T_\mu)^{abc}$, where Γ_ν is the chiral connection defined as $(X, T_\mu)^{abc} = (X)^a_d T^{dbc}_\mu + (X)^b_d T^{adc}_\mu + (X)^c_d T^{abd}_\mu$. $\gamma^{\mu\nu\alpha}$, $\gamma^{\mu\nu}$ are the antisymmetric matrices expressed as

$$
\gamma^{\mu\nu} = \frac{1}{2}[\gamma^\mu, \gamma^\nu] \quad \text{and} \quad \gamma^{\mu\nu\rho} = \frac{1}{4}\{[\gamma^\mu, \gamma^\nu], \gamma^\rho\}. \tag{4}
$$

The octet, decuplet, and octet-decuplet transition operators for magnetic moment are needed in the one-loop

calculations. The anomalous magnetic Lagrangian of octet baryons is written as

$$
\mathcal{L}_{\text{oct}} = \frac{e}{4m_B}(c_1\text{Tr}(\bar{B}\sigma^{\mu\nu}\{F^+_{\mu\nu}, B\}) + c_2\text{Tr}(\bar{B}\sigma^{\mu\nu}[F^+_{\mu\nu}, B])
$$

$$
+ c_3\text{Tr}(\bar{B}\sigma^{\mu\nu}B)\text{Tr}(F^+_{\mu\nu})), \tag{5}
$$

where

$$
F^\dagger_{\mu\nu} = -\frac{1}{2}(\zeta^\dagger F_{\mu\nu}Q_c\zeta + \zeta F_{\mu\nu}Q_c\zeta^\dagger). \tag{6}
$$

The above Lagrangian will contribute to the Pauli form factor F_2 which is defined in Eq. (19). At the lowest order, the contribution of quark q with unit charge to the octet magnetic moments can be obtained by replacing the charge matrix Q_c with the corresponding diagonal quark matrices $\lambda_q = \text{diag}(\delta_{qu}, \delta_{qd}, \delta_{qs})$. Let us take the nucleon as an example. After expansion of the above equation, it is found that

$$
F_2^{p,u} = c_1 + c_2 + c_3, \qquad F_2^{p,d} = c_3, \qquad F_2^{p,s} = c_1 - c_2 + c_3,
$$

$$
F_2^{n,u} = c_3, \qquad F_2^{n,d} = c_1 + c_2 + c_3, \qquad F_2^{n,s} = c_1 - c_2 + c_3. \tag{7}
$$

Comparing with the results of the constituent quark model where

$$F_2^{p,s} = 0 \quad \text{and} \quad F_2^{n,s} = 0, \tag{8}$$

we get

$$c_3 = c_2 - c_1. \tag{9}$$

The decuplet anomalous magnetic moment operator is expressed as

$$\mathcal{L}_{\text{dec}} = -\frac{ieF_2^T}{4M_T} \bar{T}_{\mu,abc} \sigma_{\rho\lambda} F^{\rho\lambda} T^{\mu,abc}. \tag{10}$$

The transition magnetic operator is written as

$$\mathcal{L}_{\text{trans}} = i \frac{e}{4m_B} \mu_T F_{\mu\nu} (\epsilon^{ijk} Q_{c,il} \bar{B}_{jm} \gamma^\mu \gamma_5 T^{\nu,klm}$$
$$+ \epsilon^{ijk} Q_{c,li} \bar{T}^{\mu,klm} \gamma^\nu \gamma_5 B_{mj}). \tag{11}$$

The anomalous magnetic moments of baryons can also be expressed in terms of quark magnetic moments μ_q. For example, $\mu_p = \frac{4}{3}\mu_u - \frac{1}{3}\mu_d$, $\mu_n = \frac{4}{3}\mu_d - \frac{1}{3}\mu_u$, $\mu_{\Delta^{++}} = 3\mu_u$. Using the SU(3) symmetry, $\mu_u = -2\mu_d = -2\mu_s$, μ_T and F_2^T as well as μ_q can be written in terms of c_1 or c_2. For example, $\mu_u = \frac{2}{3}c_1$, $\mu_T = 4c_1$, $F_2^{\Delta^{++}} = \mu_{\Delta^{++}} - 2 = 2c_1 - 2$.

The gauge invariant nonlocal Lagrangian can be obtained using the method in [25,26,39]. For instance, the local interaction between hyperons and K^- meson can be written as

$$\mathcal{L}_K^{\text{local}} = \frac{D+F}{\sqrt{2}f} \bar{\Xi}^0(x) \gamma^\mu \gamma_5 \Sigma^+(x) (\partial_\mu + ie\mathcal{A}_\mu(x)) K^-(x). \tag{12}$$

The corresponding nonlocal Lagrangian is expressed as

$$\mathcal{L}_K^{\text{nl}} = \int d^4 y \frac{D+F}{\sqrt{2}f} \bar{\Xi}^0(x) \gamma^\mu \gamma_5 \Sigma^+(x) \left(\partial_{x,\mu} + ie \int d^4 a \mathcal{A}_\mu(x-a) \right) F(a)$$
$$\times F(x-y) \exp\left(ie \int_x^y dz_\nu \int d^4 a \mathcal{A}^\nu(z-a) F(a) \right) K^-(y), \tag{13}$$

where $F(x)$ is the correlation function. From the Lagrangian, one can see that the meson and photon fields are displaced, while the baryon fields are still at the same point. In principle, we can also displace the baryon fields. As a result, the free baryon Lagrangian has to be nonlocal in order to make the total Lagrangian gauge invariant. Therefore the baryon propagator and quantization will be modified. The general version of this nonlocal chiral Lagrangian is much more complicated. In this paper, we do not change the free Lagrangian and only the interacting Lagrangian is nonlocal. To guarantee gauge invariance, the gauge link $\exp(ie \int_x^y dz_\nu \int d^4 a \mathcal{A}^\nu(z-a) F(a)) K^-(y)$ is introduced to the above Lagrangian. The photon can be emitted or annihilated from the minimal substitution term or gauge link term. The correlation function is associated with each photon field or meson field. With the correlation function, the regulator and form factors at tree level can be generated automatically. In the numerical calculation, the correlation function is chosen to be a dipole form in momentum space.

The nonlocal baryon-photon interaction can also be obtained in the same procedure. For example, the local interaction between Σ^+ and the photon is written as

$$\mathcal{L}_{\text{EM}}^{\text{local}} = -e\bar{\Sigma}^+(x) \gamma^\mu \Sigma^+(x) \mathcal{A}_\mu(x)$$
$$+ \frac{(c_1 + 3c_2)e}{12m_\Sigma} \bar{\Sigma}^+(x) \sigma^{\mu\nu} \Sigma(x)^+ F_{\mu\nu}(x). \tag{14}$$

The corresponding nonlocal Lagrangian is expressed as

$$\mathcal{L}_{\text{EM}}^{\text{nl}} = -e \int d^4 a \bar{\Sigma}^+(x) \gamma^\mu \Sigma(x)^+ \mathcal{A}_\mu(x-a) F_1(a)$$
$$+ \frac{(c_1 + 3c_2)e}{12m_\Sigma}$$
$$\times \int d^4 a \bar{\Sigma}^+(x) \sigma^{\mu\nu} \Sigma(x)^+ F_{\mu\nu}(x-a) F_2(a), \tag{15}$$

where $F_1(a)$ and $F_2(a)$ are the correlation functions for the nonlocal electric and magnetic interactions.

The momentum dependence of the form factors at tree level can be easily obtained with the Fourier transformation of the correlation function. As in our previous work [25,26], the correlation function is chosen such that the charge and magnetic form factors at tree level have the same momentum dependence as the baryon-meson vertex, i.e., $G_M^{B,\text{tree}}(q) = \mu_B G_E^{B,\text{tree}}(q) = \mu_B \tilde{F}(q)$, where $\tilde{F}(q)$ is the Fourier transformation of the correlation function $F(a)$. Therefore, the corresponding functions $\tilde{F}_1(q)$ and $\tilde{F}_2(q)$ of Σ^+, for example, are expressed as

$$\tilde{F}_1^{\Sigma^+}(q) = \tilde{F}(q) \frac{12m_\Sigma^2 + (3 + c_1 + 3c_2)Q^2}{3(4m_\Sigma^2 + Q^2)},$$

$$\tilde{F}_2^{\Sigma^+}(q) = \tilde{F}(q) \frac{4(c_1 + 3c_2)m_\Sigma^2}{3(4m_\Sigma^2 + Q^2)}, \tag{16}$$

where $Q^2 = -q^2$ is the momentum transfer. From Eq. (13), two kinds of couplings between hadrons and photons can be obtained. One is the normal coupling, expressed as

$$\mathcal{L}^{\text{norm}} = ie \int d^4y \frac{D+F}{\sqrt{2}f} \bar{\Xi}^0(x)\gamma^\mu\gamma_5\Sigma^+(x)$$
$$\times \int d^4 a \mathcal{A}_\mu(x-a)F(a)F(x-y)K^-(y). \quad (17)$$

This interaction is similar to the traditional local Lagrangian except for the correlation function. The other is the additional interaction obtained by the expansion of the gauge link, expressed as

$$\mathcal{L}^{\text{add}} = ie \int d^4y \frac{D+F}{\sqrt{2}f} \bar{\Xi}^0(x)\gamma^\mu\gamma_5\Sigma^+(x)\partial_{x,\mu}\left(F(x-y)\right.$$
$$\left.\times \int_x^y dz_\nu \int d^4 a \mathcal{A}^\nu(z-a)F(a)K^-(y)\right). \quad (18)$$

The additional interaction guarantees the charge conservation.

The Dirac and Pauli form factors of octet baryons are defined as

$$\langle B(p')|J^\mu|B(p)\rangle$$
$$= \bar{u}(p')\left\{\gamma^\mu F_1^B(Q^2) + \frac{i\sigma^{\mu\nu}q_\nu}{2m_B}F_2^B(Q^2)\right\}u(p), \quad (19)$$

where $q = p' - p$. The electromagnetic form factors are defined as the combinations of the above form factors as

$$G_E^B(Q^2) = F_1^B(Q^2) - \frac{Q^2}{4m_B^2}F_2^B(Q^2),$$
$$G_M^B(Q^2) = F_1^B(Q^2) + F_2^B(Q^2). \quad (20)$$

With the electromagnetic form factors, the magnetic and electric (charge) radii can be obtained. The magnetic radii of octet baryons are defined as

$$\langle r_M^2\rangle_B = \frac{-6}{G_M^B(0)}\frac{dG_M^B(Q^2)}{dQ^2}\bigg|_{Q^2=0}. \quad (21)$$

The electric radii of charged and neutral baryons are defined as

$$\langle r_E^2\rangle_B = \frac{-6}{G_E^B(0)}\frac{dG_E^B(Q^2)}{dQ^2}\bigg|_{Q^2=0} \quad \text{and}$$
$$\langle r_E^2\rangle_B = -6\frac{dG_E^B(Q^2)}{dQ^2}\bigg|_{Q^2=0}, \quad (22)$$

respectively.

According to the Lagrangian, the one-loop Feynman diagrams which contribute to the octet electromagnetic form factors are shown in Fig. 1. From the Lagrangian, we can get the matrix element of Eq. (19). The π meson loops have the dominant contributions, while the contributions from K meson loops are much smaller due to the large K meson mass. The contributions from η and η' loops are even smaller which are neglected in our calculation. The inclusion of these mesons does not affect the main conclusion. The expressions for the intermediate octet and decuplet baryons are written in the Appendix. In the next section, we will discuss the numerical results.

III. NUMERICAL RESULTS

The coupling constants between octet baryons and mesons are determined by the two parameters D and F. In the numerical calculations, the parameters are chosen as $D = 0.76$ and $F = 0.50$ ($g_A = D + F = 1.26$) [40]. The coupling constant $\mathcal{C}$ is chosen to be $2D$ which is the same as in Refs. [40,41]. The off-shell parameter z is -1 [42]. The physical masses are taken for mesons, octet, and decuplet baryons. The covariant regulator is chosen to be the dipole form [25–27]

$$\tilde{F}(k) = \frac{\Lambda^4}{(k^2 - m_j^2 - \Lambda^2)^2}, \quad (23)$$

where m_j is the meson mass for the baryon-meson interaction and it is zero for the hadron-photon interaction. It was found that when Λ was around 0.90 GeV, the obtained nucleon form factors were very close to the experimental data. Therefore, all of the above parameters are predetermined. There are only two free parameters which are the low-energy constants (LECs) c_1 and c_2. In our previous calculation for the nucleon form factors, they were fitted to the experimental nucleon magnetic moments [25]. Here, c_1 and c_2 are determined to be 1.288 and 0.420, which give the minimal χ^2 of the octet magnetic moments.

In Table I, the tree, loop, and total contributions to the baryon magnetic moments obtained from the nonlocal chiral effective theory are listed. The wave-function renormalization constant Z is included in the calculation, i.e., the tree-level contribution has been multiplied by Z. The error bar in our calculation is determined by varying Λ from 0.8 to 1.0 GeV. The results from two lattice simulations [30,31], ChPT with IR [33] and EOMS scheme [36], NJL and PCQM models [43,44] as well as the experimental data are also listed for comparison. From the table, one can see that all the magnetic moments of octet baryons are reasonably reproduced. The largest deviation from the experiments is for Ξs, where the calculated central values of magnetic moments of μ_{Ξ^0} and μ_{Ξ^-} are about 10% larger than experimental ones. For the other baryons, the deviation from the experiments is less than 5%.
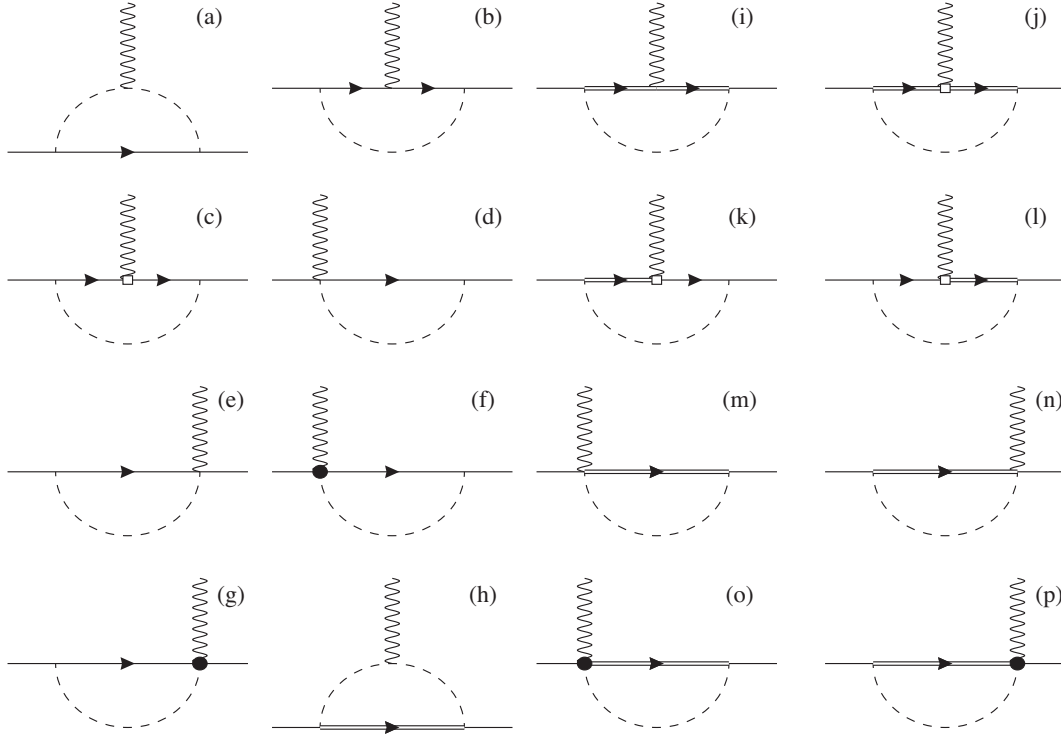
FIG. 1.   One-loop Feynman diagrams for the octet electromagnetic form factors. The solid, double-solid, dashed, and wave lines are for the octet baryons, decuplet baryons, pseudoscalar mesons, and photons, respectively. The rectangle and black dot represent magnetic and additional interacting vertex.

Considering the error bar, the calculated magnetic moments of octet baryons are in very good agreement with the experimental values. It is interesting that all the tree and loop contributions have the same signs except for Ξ^-, where the loop diagrams give the opposite contribution to the tree diagram. The data from lattice simulations are somewhat smaller which is partially due to the large pion mass and/or the neglecting of the disconnected contribution. The results at order of $\mathcal{O}(p^3)$ in ChPT with IR are listed for comparison, where the calculated moments of most baryons are comparable with the experimental data. The magnetic moment of Ξ^- is about 40%–50% larger which could be decreased by the inclusion of intermediate decuplet states. At order of $\mathcal{O}(p^4)$, with the additional five

low-energy constants, the seven experimental magnetic moments can be exactly reproduced [33]. For the ChPT with EOMS scheme, the results with the inclusion of intermediate decuplet states and vector mesons are listed. It was found that the inclusion of intermediate decuplet states improves the results, especially for Ξ^- and makes the results at $\mathcal{O}(p^3)$ as good as those at $\mathcal{O}(p^4)$ [36]. Our calculation in nonlocal EFT confirms that the results at one-loop level with the inclusion of decuplet states are good enough to reproduce the experimental values.

The magnetic form factors of charged octet baryons versus momentum transfer Q^2 are plotted in Fig. 2. The solid, dashed, dotted, and dash-dotted lines are for proton, Σ^+, Σ^-, and Ξ^-, respectively. The magnetic form factor of

TABLE I.   The tree, loop and total contributions to the octet magnetic moments μ_B (in units of the nucleon magneton μ_N). The results from two lattice simulations, ChPT with IR and EOMS scheme, NJL and PCQM models as well as the experimental data are also listed.

|	Tree	Loop	Total	Lattice [45]	Lattice [31]	ChPT[33]	ChPT[36]	NJL [43]	PCQM [44]	Experimental [46]
μ_p	1.850	0.795	2.644 ± 0.159	2.4(2)	2.3(3)	2.61	2.79	2.78	2.735 ± 0.121	2.793
μ_n	-0.859	-1.126	-1.984 ± 0.216	$-1.59(17)$	$-1.45(17)$	-1.69	-1.913	-1.81	-1.956 ± 0.103	-1.913
μ_{Σ^+}	1.850	0.572	2.421 ± 0.147	2.27(16)	2.12(18)	2.53	2.1(4)	2.62	2.537 ± 0.201	2.458 ± 0.010
μ_{Σ^0}	0.429	0.155	0.584 ± 0.077	…	…	0.76	0.5(2)	…	0.838 ± 0.091	…
μ_{Σ^-}	-0.991	-0.262	-1.253 ± 0.008	$-0.88(8)$	$-0.85(10)$	-1.00	$-1.1(1)$	-1.62	-0.861 ± 0.040	-1.160 ± 0.025
μ_Λ	-0.429	-0.165	-0.594 ± 0.057	…	…	-0.76	$-0.5(2)$	…	-0.867 ± 0.074	-0.613 ± 0.004
μ_{Ξ^0}	-0.859	-0.521	-1.380 ± 0.169	$-1.32(4)$	$-1.07(7)$	-1.51	$-1.0(4)$	-1.14	-1.690 ± 0.142	-1.250 ± 0.014
μ_{Ξ^-}	-0.991	0.266	-0.725 ± 0.077	$-0.71(3)$	$-0.57(5)$	-0.93	$-0.7(1)$	-0.67	-0.840 ± 0.087	-0.651 ± 0.080
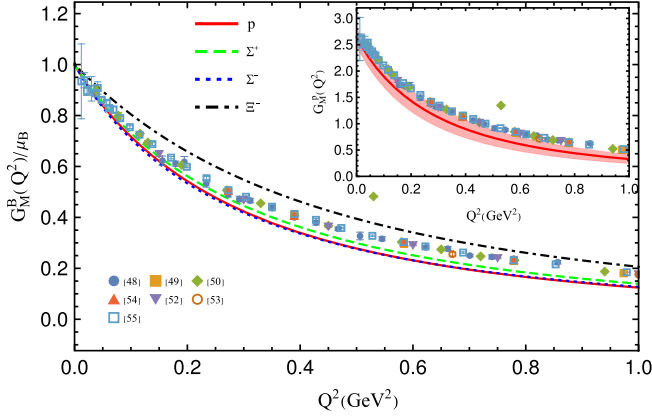
FIG. 2. The normalized magnetic form factors of charged octet baryons G_M^B/μ_B versus momentum transfer Q^2. The solid, dashed, dotted, and dash-dotted lines are for proton, Σ^+, Σ^-, and Ξ^-, respectively. The magnetic form factor of proton with Λ varying from 0.8 to 1 GeV is also plotted at the corner of the figure. The experimental form factor of the proton is from Refs. [48–55].
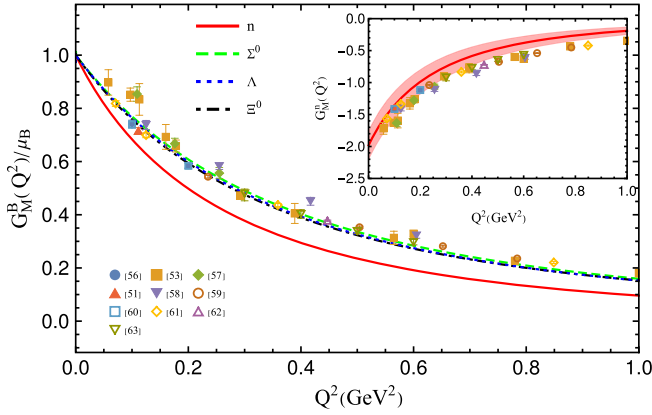

FIG. 3. The normalized magnetic form factors of neutral octet baryons G_M^B/μ_B versus momentum transfer Q^2. The solid, dashed, dotted, and dash-dotted lines are for neutron, Σ^0, Λ, and Ξ^0, respectively. The magnetic form factor of the neutron with Λ varying from 0.8 to 1 GeV is also plotted at the corner of the figure. The experimental form factor of the neutron is from Refs. [51,53,56–63].

the proton with Λ varying from 0.8 to 1 GeV is also plotted at the corner of the figure. Considering the error bar, it is clear the proton magnetic form factor is comparable with the experimental data up to 1 GeV^2. This is the advantage of the nonlocal chiral effective theory. The correlation function in the nonlocal Lagrangian makes the loop integral convergent. In the mean time, it provides the momentum dependence of the form factors at tree level, and as a result, the total form factors can be close to the experimental data up to relatively large Q^2. The normalized magnetic form factors of the nucleon were studied in the chiral perturbation theory including ρ and ω mesons as well as the Δ resonance [47]. Two of the undetermined low-energy coupling constants were adjusted to the nucleon magnetic moments while the remaining six LECs were fitted simultaneously to the experimental data up to $Q^2 = 0.4$ GeV^2. It was found that the results incorporating vector mesons agree well with experimental data in a momentum transfer region $0 \leq Q^2 \leq 0.4$ GeV^2. The other form factors of charged baryons have a similar momentum dependence as the proton. Among them, Ξ^- decreases a little slower with increasing Q^2. The magnetic radii are determined by the slopes of the form factors at zero momentum transfer which will be discussed later.

The normalized magnetic form factors for the charge neutral baryons are plotted in Fig. 3. The solid, dashed, dotted, and dash-dotted lines are for neutron, Σ^0, Λ, and Ξ^0, respectively. The band in the small figure is for the magnetic form factor of the neutron with Λ varying from 0.8 to 1 GeV. The magnetic from factors of Σ^0, Λ, and Ξ^0 are close to each other. The normalized neutron magnetic form factor is a little smaller than the experimental data and it drops faster than the other three neutral baryons. Taking the error bar into account, the calculated neutron magnetic form factor is still close to the experiments. The smaller normalized magnetic form factor of the neutron is partially because of its larger calculated moment. All of the form factors of octet baryons have a dipolelike momentum dependence.

The tree, loop, and total contributions to the magnetic radii of octet baryons are listed in Table II. The data

TABLE II. The tree, loop, and total contributions to the octet magnetic radii $\langle r_M^2 \rangle_B$ (in units of fm^2). The results from two lattice simulations, ChPT with IR and EOMS scheme, NJL and PCQM models as well as the experimental data are also listed.

|	Tree	Loop	Total	Lattice [30]	Lattice [31]	ChPT[33]	ChPT[36]	NJL [43]	PCQM [44]	Experimental [46]
$\langle r_M^2 \rangle_p$	0.403	0.382	0.785 ± 0.132	0.470(48)	0.71(8)	0.699	0.9(2)	0.76	0.909 ± 0.084	0.72 ± 0.04
$\langle r_M^2 \rangle_n$	0.250	0.596	0.845 ± 0.148	0.478(50)	0.86(9)	0.790	0.8(2)	0.83	0.922 ± 0.079	0.75 ± 0.02
$\langle r_M^2 \rangle_{\Sigma^+}$	0.441	0.324	0.765 ± 0.131	0.466(42)	0.66(5)	0.80 ± 0.05	1.2(2)	0.77	0.885 ± 0.094	$\cdots$
$\langle r_M^2 \rangle_{\Sigma^0}$	0.424	0.194	0.618 ± 0.124	0.432(38)	$\ldots$	0.45 ± 0.08	1.1(2)	$\ldots$	0.851 ± 0.102	$\ldots$
$\langle r_M^2 \rangle_{\Sigma^-}$	0.456	0.445	0.901 ± 0.119	0.483(49)	1.05(9)	1.20 ± 0.13	1.2(2)	0.92	0.951 ± 0.083	$\ldots$
$\langle r_M^2 \rangle_{\Lambda}$	0.417	0.203	0.620 ± 0.126	0.347(24)	$\ldots$	0.48 ± 0.09	0.6(2)	$\ldots$	0.852 ± 0.103	$\ldots$
$\langle r_M^2 \rangle_{\Xi^0}$	0.359	0.298	0.657 ± 0.128	0.384(22)	0.53(5)	0.61 ± 0.12	0.7(3)	0.44	0.871 ± 0.099	$\ldots$
$\langle r_M^2 \rangle_{\Xi^-}$	0.789	-0.255	0.534 ± 0.135	0.336(18)	0.44(5)	0.50 ± 0.16	0.8(1)	0.26	0.840 ± 0.109	$\ldots$
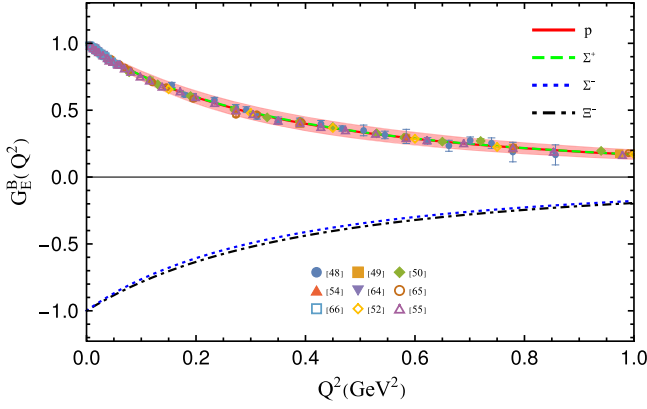
FIG. 4. Same as Fig. 2 but for electric form factors. The experimental form factor of the proton is from Refs. [48–50,52,54,55,64–66].
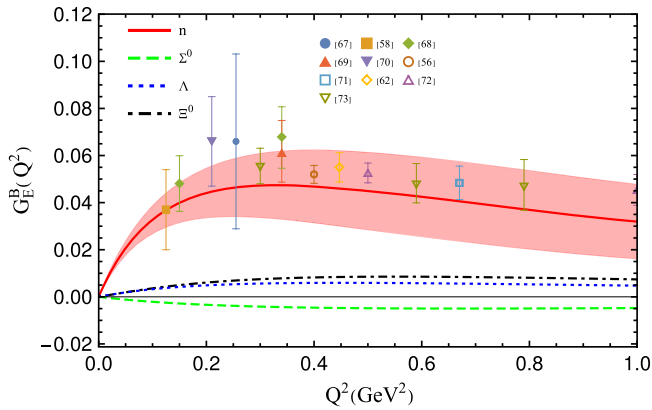

FIG. 5. Same as Fig. 3 but for electric form factors. The experimental form factor of the neutron is from Refs. [56,58,62,67–73].

from lattice simulation, chiral perturbation theory, and phenomenological quark models are also listed for comparison. Although our central values for protons and neutrons are a little larger than experiments, the results are still reasonable. The magnetic radii of octet baryons vary from 0.5 fm^2 to 0.9 fm^2, but show no simple

dependence on baryon/quark mass. Ξ^- has the largest contribution at tree level. Because of the opposite contribution from the loop diagrams, its total radius is the smallest one. The amazing thing is although the values from different methods are quite different, the order of the values from the largest to smallest is almost the same. For example, Σ^- and Ξ^- have the largest and smallest magnetic radii, respectively. The neutron magnetic radius is the second largest one. Our results also show the tree and loop contributions are strongly baryon dependent. The loop contribution to $\langle r_M^2 \rangle_{\Sigma^0}$ is less than one half of the tree contribution. However, for neutron, the loop contribution is twice as big as the tree contribution.

We now discuss the electric form factors. Similar as for magnetic form factors, the bands are also shown for nucleon electric form factors with 0.8 GeV $\leq \Lambda \leq$ 1 GeV. In Fig. 4, we plot the electric form factors of the charged baryons. Because of the additional interaction which makes the nonlocal Lagrangian locally gauge invariant, the electric form factors start from their charge at $Q^2 = 0$. The proton charge form factor is close to the experimental data. The absolute values of the electric form factors of charged baryons have a similar momentum dependence. This could be examined by the further experiments and/or accurate lattice simulation.

The electric form factors for the neutral baryons are plotted in Fig. 5. Again due to the charge conservation, the form factors start from 0 at zero momentum transfer. The calculated electric form factor of the neutron is consistent with the experimental data. The form factors of the other neutral baryons are very small. There is no tree level contribution to the electric form factors of neutral baryons and all the contributions are from the loop diagrams. Among them, the neutron has the largest contribution from π-loop diagrams. The corresponding π-loop diagrams for the other neutral baryons are fairy small due to the small coupling constants.

The charge radii of octet baryons are listed in Table III. Our results are comparable with the experimental data in PDG for nucleon and Σ^-. A small proton charge radius $\langle r_E \rangle_p = 0.831 \pm 0.007 \pm 0.012$, i.e., $\langle r_E^2 \rangle_p = 0.691 \pm 0.032$

TABLE III. The tree, loop, and total contributions to the octet charge radii $\langle r_E^2 \rangle_B$ (in units of fm^2). The results from two lattice simulations, ChPT with IR and EOMS scheme, NJL and PCQM models as well as the experimental data are also listed.

	Tree	Loop	Total	Lattice[24]	Lattice[32]	ChPT[33]	ChPT[36]	NJL[43]	PCQM [44]	Experimental [46]
$\langle r_E^2 \rangle_p$	0.577	0.152	0.729 ± 0.112	0.685(66)	0.76(10)	0.717	0.878	0.76	0.767 ± 0.113	0.707 ± 0.0007
$\langle r_E^2 \rangle_n$	0	-0.146	-0.146 ± 0.018	$-0.158(33)$	$\cdots$	-0.113	0.03(7)	-0.14	-0.014 ± 0.001	-0.116 ± 0.0022
$\langle r_E^2 \rangle_{\Sigma^+}$	0.577	0.142	0.719 ± 0.116	0.749(72)	0.61(8)	0.60 ± 0.02	0.99(3)	0.92	0.781 ± 0.108	$\cdots$
$\langle r_E^2 \rangle_{\Sigma^0}$	0	0.010	0.010 ± 0.004	$\cdots$	$\cdots$	-0.03 ± 0.01	0.10(2)	$\cdots$	0	$\cdots$
$\langle r_E^2 \rangle_{\Sigma^-}$	0.577	0.123	0.700 ± 0.124	0.657(58)	0.45(3)	0.67 ± 0.03	0.780	0.74	0.781 ± 0.063	0.61 ± 0.16
$\langle r_E^2 \rangle_{\Lambda}$	0	-0.015	-0.015 ± 0.004	0.010(9)	$\cdots$	0.11 ± 0.02	0.18(1)	$\cdots$	0	$\cdots$
$\langle r_E^2 \rangle_{\Xi^0}$	0	-0.015	-0.015 ± 0.007	0.082(29)	$\cdots$	0.13 ± 0.03	0.36(2)	0.24	0.014 ± 0.008	$\cdots$
$\langle r_E^2 \rangle_{\Xi^-}$	0.577	0.025	0.601 ± 0.127	0.502(47)	0.37(2)	0.49 ± 0.05	0.61(1)	0.58	0.767 ± 0.113	$\cdots$

was reported recently [3] which is also close to our value $\langle r_E^2 \rangle_p = 0.729 \pm 0.112$. For the neutral baryons, the loop contribution is very small except that of the neutron. For the charged baryons, the tree level contributions are the same which are also dominant for all of them. The loop contribution has the same order of magnitude except for Ξ^-, where the loop contribution is small. Different from the magnetic radii, the total charge radii vary around 0.6 and 0.7 fm^2 for the charged baryons. Although the charge radii of charged baryons from different models are comparable, the predictions for neutral baryons (both sign and size) are quite different.

IV. SUMMARY

We applied the nonlocal chiral effective theory to study the electromagnetic form factors of octet baryons. The correlation function in the Lagrangian makes the loop integral convergent. It also provides the momentum dependence of the form factors at tree level. The additional interaction generated from the expansion of the gauge link guarantees the Lagrangian is locally gauge invariant. This nonlocal Lagrangian makes it possible to study the physical quantities at relatively large momentum transfer in the framework of chiral effective theory. In the numerical calculation, all the parameters are predetermined except the two low-energy constants c_1 an c_2. They are fitted to give the minimum of χ^2 of the octet magnetic moments. When extending the previous study of form factors of nucleons to all the octet baryons, we do not add any new parameter. The magnetic moments are well reproduced. The deviation from the experiments is less than 5% except Ξ^0 and Ξ^-, where the deviation of the central value is about 10%. For the radii, most experiments focus on the nucleon and there is few data for the other baryons. Considering the error bar, all our results on magnetic moments and electromagnetic radii are in very good agreement with the current experimental data. The calculated nucleon form factors are close to the experiments up to $Q^2 = 1$ GeV^2. For the other octet baryons, since the method is the same, we expect this nonlocal Lagrangian can also give good descriptions. The difference between our results and those

of other theoretical methods could be examined by future experiments and more accurate lattice simulations.

APPENDIX: LOOP EXPRESSIONS

In this section, we show the expressions of loop integrals for the intermediate octet and decuplet baryons. Let us take the Σ hyperons as an example.

The contributions of Fig. 1(a) are written as

$$\Gamma_a^\mu(\Sigma^-) = \frac{F^2}{f^2} I_a^{\mu,\Sigma\pi} + \frac{D^2}{3f^2} I_a^{\mu,\Lambda\pi} + \frac{(D-F)^2}{2f^2} I_a^{\mu,NK}, \quad (A1)$$

$$\Gamma_a^\mu(\Sigma^0) = \frac{(D-F)^2}{4f^2} I_a^{\mu,NK} - \frac{(D+F)^2}{4f^2} I_a^{\mu,\Xi K}, \quad (A2)$$

$$\Gamma_a^\mu(\Sigma^+) = -\frac{F^2}{f^2} I_a^{\mu,\Sigma\pi} - \frac{D^2}{3f^2} I_a^{\mu,\Lambda\pi} - \frac{(D+F)^2}{2f^2} I_a^{\mu,\Xi K}, \quad (A3)$$

where the integral $I_a^{\mu,BM}$ is expressed as

$$I_a^{\mu,BM} = \bar{u}(p')\tilde{F}(q) \int \frac{\mathrm{d}^4 k}{(2\pi)^4} \frac{\tilde{F}(q+k)\tilde{F}(k)}{D_M(k+q)} \frac{-(2k+q)^\mu}{D_M(k)}$$
$$\times (\slashed{k} + \slashed{q})\gamma_5 \frac{1}{\slashed{p} - \slashed{k} - m_B} \slashed{k}\gamma_5 u(p). \quad (A4)$$

$D_M(k)$ is defined as

$$D_M(k) = k^2 - m_M^2 + i\epsilon. \quad (A5)$$

m_B and m_M are the masses of the intermediate B baryon and M meson.

The contributions of Fig. 1(b) are expressed as

$$\Gamma_b^\mu(\Sigma^-) = \frac{F(c_1 D Q^2 - F((-2c_1 + 3c_2 + 3)Q^2 + 12m_\Sigma^2))}{3f^2(4m_\Sigma^2 + Q^2)} I_b^{\mu,\Sigma\pi} - \frac{c_1 D Q^2(D-3F)}{9f^2(4m_\Lambda^2 + Q^2)} I_b^{\mu,\Lambda\pi}$$
$$- \frac{c_1 Q^2(D-F)^2}{3f^2(4m_N^2 + Q^2)} I_b^{\mu,NK} - \frac{(D+F)^2((-c_1 + 3c_2 + 3)Q^2 + 12m_\Xi^2)}{6f^2(4m_\Xi^2 + Q^2)} I_b^{\mu,\Xi K}, \quad (A6)$$

$$\Gamma_b^\mu(\Sigma^0) = \frac{2c_1 F^2 Q^2}{3f^2(4m_\Sigma^2 + Q^2)} I_b^{\mu,\Sigma\pi} - \frac{c_1 D^2 Q^2}{9f^2(4m_\Lambda^2 + Q^2)} I_b^{\mu,\Lambda\pi} + \frac{(D-F)^2((-c_1 + 3c_2 + 3)Q^2 + 12m_N^2)}{12f^2(4m_N^2 + Q^2)} I_b^{\mu,NK}$$
$$- \frac{(D+F)^2((c_1 + 3c_2 + 3)Q^2 + 12m_\Xi^2)}{12f^2(4m_\Xi^2 + Q^2)} I_b^{\mu,\Xi K}, \quad (A7)$$

$$\Gamma_b^\mu(\Sigma^+) = \frac{F(c_1(-D)Q^2 + (2c_1 + 3c_2 + 3)FQ^2 + 12Fm_\Sigma^2)}{3f^2(4m_\Sigma^2 + Q^2)} I_b^{\mu,\Sigma\pi} - \frac{c_1 DQ^2(D + 3F)}{9f^2(4m_\Lambda^2 + Q^2)} I_b^{\mu,\Lambda\pi}$$

$$+ \frac{(D-F)^2((c_1 + 3c_2 + 3)Q^2 + 12m_N^2)}{6f^2(4m_N^2 + Q^2)} I_b^{\mu,NK} - \frac{c_1 Q^2(D+F)^2}{3f^2(4m_\Xi^2 + Q^2)} I_b^{\mu,\Xi K}, \tag{A8}$$

where the integral $I_b^{\mu,BM}$ is written as

$$I_b^{\mu,BM} = \bar{u}(p')\tilde{F}(q) \int \frac{\mathrm{d}^4 k}{(2\pi)^4} \frac{\tilde{F}(k)^2}{D_M(k)} \slashed{k}\gamma_5 \frac{1}{\slashed{p}' - \slashed{k} - m_B} \gamma^\mu \frac{1}{\slashed{p} - \slashed{k} - m_B} \slashed{k}\gamma_5 u(p). \tag{A9}$$

Figure 1(c) is similar to Fig. 1(b) except for the magnetic interaction. The contributions of this diagram are written as

$$\Gamma_c^\mu(\Sigma^-) = \frac{2Fm_\Sigma(c_1(D + 2F) - 3c_2 F)}{3f^2(4m_\Sigma^2 + Q^2)} I_c^{\mu,\Sigma\pi}$$

$$- \frac{2c_1 D(D - 3F)m_\Lambda}{9f^2(4m_\Lambda^2 + Q^2)} I_c^{\mu,\Lambda\pi}$$

$$- \frac{2c_1(D - F)^2 m_N}{3f^2(4m_N^2 + Q^2)} I_c^{\mu,NK}$$

$$+ \frac{(c_1 - 3c_2)(D + F)^2 m_\Xi}{3f^2(4m_\Xi^2 + Q^2)} I_c^{\mu,\Xi K}, \tag{A10}$$

$$\Gamma_c^\mu(\Sigma^0) = \frac{4c_1 F^2 m_\Sigma}{3f^2(4m_\Sigma^2 + Q^2)} I_c^{\mu,\Sigma\pi} - \frac{2c_1 D^2 m_\Lambda}{9f^2(4m_\Lambda^2 + Q^2)} I_c^{\mu,\Lambda\pi}$$

$$- \frac{(c_1 - 3c_2)(D - F)^2 m_N}{6f^2(4m_N^2 + Q^2)} I_c^{\mu,NK}$$

$$- \frac{(c_1 + 3c_2)(D + F)^2 m_\Xi}{6f^2(4m_\Xi^2 + Q^2)} I_c^{\mu,\Xi K}, \tag{A11}$$

$$\Gamma_c^\mu(\Sigma^+) = \frac{2Fm_\Sigma(c_1(-D) + 2c_1 F + 3c_2 F)}{3f^2(4m_\Sigma^2 + Q^2)} I_c^{\mu,\Sigma\pi}$$

$$- \frac{2c_1 D(D + 3F)m_\Lambda}{9f^2(4m_\Lambda^2 + Q^2)} I_c^{\mu,\Lambda\pi}$$

$$+ \frac{(c_1 + 3c_2)(D - F)^2 m_N}{3f^2(4m_N^2 + Q^2)} I_c^{\mu,NK}$$

$$- \frac{2c_1(D + F)^2 m_\Xi}{3f^2(4m_\Xi^2 + Q^2)} I_c^{\mu,\Xi K}, \tag{A12}$$

where $I_c^{\mu,BM}$ is expressed as

$$I_c^{\mu,BM} = \bar{u}(p')\tilde{F}(q) \int \frac{\mathrm{d}^4 k}{(2\pi)^4} \frac{\tilde{F}(k)^2}{D_M(k)} \slashed{k}\gamma_5 \frac{1}{\slashed{p} - \slashed{k} - m_B} i\sigma^{\mu\nu} q_\nu$$

$$\times \frac{1}{\slashed{p} - \slashed{k} - m_B} \slashed{k}\gamma_5 u(p). \tag{A13}$$

Figures 1(d) and 1(e) are the Kroll-Ruderman diagrams. The contributions of these two diagrams are written as

$$\Gamma_{d+e}^\mu(\Sigma^-) = \frac{F^2}{f^2} I_{d+e}^{\mu,\Sigma\pi} + \frac{D^2}{3f^2} I_{d+e}^{\mu,\Lambda\pi} + \frac{(D-F)^2}{2f^2} I_{d+e}^{\mu,NK}, \tag{A14}$$

$$\Gamma_{d+e}^\mu(\Sigma^0) = \frac{(D-F)^2}{4f^2} I_{d+e}^{\mu,NK} - \frac{(D+F)^2}{4f^2} I_{d+e}^{\mu,\Xi K}, \tag{A15}$$

$$\Gamma_{d+e}^\mu(\Sigma^+) = -\frac{F^2}{f^2} I_{d+e}^{\mu,\Sigma\pi} - \frac{D^2}{3f^2} I_{d+e}^{\mu,\Lambda\pi} - \frac{(D+F)^2}{2f^2} I_{d+e}^{\mu,\Xi K}, \tag{A16}$$

where

$$I_{d+e}^{\mu,BM} = \bar{u}(p')\tilde{F}(q) \int \frac{\mathrm{d}^4 k}{(2\pi)^4} \frac{\tilde{F}(k)^2}{D_M(k)} \left\{ \slashed{k}\gamma_5 \frac{1}{\slashed{p}' - \slashed{k} - m_B} \gamma^\mu \gamma_5 \right.$$

$$\left. + \gamma^\mu \gamma_5 \frac{1}{\slashed{p} - \slashed{k} - m_B} \slashed{k}\gamma_5 \right\} u(p). \tag{A17}$$

Figures 1(f) and 1(g) are the additional diagrams which are generated from the expansion of the gauge link terms. The contributions of these two diagrams for intermediate octet hyperons are expressed as

$$\Gamma_{f+g}^\mu(\Sigma^-) = \frac{F^2}{f^2} I_{f+g}^{\mu,\Sigma\pi} + \frac{D^2}{3f^2} I_{f+g}^{\mu,\Lambda\pi} + \frac{(D-F)^2}{2f^2} I_{f+g}^{\mu,NK}, \tag{A18}$$

$$\Gamma_{f+g}^\mu(\Sigma^0) = \frac{(D-F)^2}{4f^2} I_{f+g}^{\mu,NK} - \frac{(D+F)^2}{4f^2} I_{f+g}^{\mu,\Xi K}, \tag{A19}$$

$$\Gamma_{f+g}^\mu(\Sigma^+) = -\frac{F^2}{f^2} I_{f+g}^{\mu,\Sigma\pi} - \frac{D^2}{3f^2} I_{f+g}^{\mu,\Lambda\pi} - \frac{(D+F)^2}{2f^2} I_{f+g}^{\mu,\Xi K}, \tag{A20}$$

where

$$I_{f+g}^{\mu,BM} = \bar{u}(p')\tilde{F}(q)\int \frac{d^4k}{(2\pi)^4}\frac{\tilde{F}(k)}{D_M(k)}\left\{\frac{(2k-q)^\mu}{2kq-q^2}[\tilde{F}(k-q)-\tilde{F}(k)]\not{k}\gamma_5\frac{1}{\not{p}'-\not{k}-m_B}(-\not{k}+\not{q})\gamma_5\right.$$
$$\left.+\frac{(2k+q)^\mu}{2kq+q^2}[\tilde{F}(k+q)-\tilde{F}(k)](\not{k}+\not{q})\gamma_5\frac{1}{\not{p}-\not{k}-m_B}\not{k}\gamma_5\right\}u(p). \tag{A21}$$

Now we show the expressions of one-loop integrals for decuplet intermediate states. The contribution for Fig. 1(h) can be written as

$$\Gamma_h^\mu(\Sigma^-) = \frac{\mathcal{C}^2}{12f^2}I_h^{\mu,\Sigma^*\pi}+\frac{\mathcal{C}^2}{6f^2}I_h^{\mu,\Delta K}, \tag{A22}$$

$$\Gamma_h^\mu(\Sigma^0) = -\frac{\mathcal{C}^2}{12f^2}I_h^{\mu,\Sigma^*\pi}+\frac{\mathcal{C}^2}{3f^2}I_h^{\mu,\Delta K}, \tag{A23}$$

$$\Gamma_h^\mu(\Sigma^+) = -\frac{\mathcal{C}^2}{12f^2}I_h^{\mu,\Sigma^*\pi}-\frac{\mathcal{C}^2}{6f^2}I_h^{\mu,\Xi^*\pi}+\frac{\mathcal{C}^2}{2f^2}I_h^{\mu,\Delta K}, \tag{A24}$$

where the integral $I_h^{\mu,TM}$ is expressed as

$$I_h^{\mu,TM} = \bar{u}(p')\tilde{F}(q)\int\frac{d^4k}{(2\pi)^4}\frac{\tilde{F}(q+k)\tilde{F}(k)}{D_M(k)}\frac{2(k+q)^\mu}{D_M(q+k)} \tag{A25}$$

$$\times((k+q)^\sigma+z(\not{k}+\not{q})\gamma^\sigma)\frac{1}{\not{p}-\not{k}-m_T}$$
$$\times S_{\sigma\rho}(p-k)(-k^\rho-z\gamma^\rho\not{k})u(p). \tag{A26}$$

m_T is the mass of the decuplet intermediate state and $S_{\sigma\rho}(p)$ is expressed as

$$S_{\sigma\rho}(p) = -g_{\sigma\rho}+\frac{\gamma_\sigma\gamma_\rho}{3}+\frac{p_\sigma p_\rho}{3m_T^2}+\frac{\gamma_\sigma p_\rho-\gamma_\rho p_\sigma}{3m_T}. \tag{A27}$$

The contribution for Fig. 1(i) is written as

$$\Gamma_i^\mu(\Sigma^-) = -\frac{\mathcal{C}^2((c_1+3c_2+3)Q^2+12m_{\Sigma^*}^2)}{36f^2(4m_{\Sigma^*}^2+Q^2)}I_i^{\mu,\Sigma^*\pi}$$
$$-\frac{\mathcal{C}^2((c_1+3c_2+3)Q^2+12m_\Delta^2)}{6f^2(4m_\Delta^2+Q^2)}I_i^{\mu,\Delta K}$$
$$-\frac{\mathcal{C}^2((c_1+3c_2+3)Q^2+12m_{\Xi^*}^2)}{18f^2(4m_{\Xi^*}^2+Q^2)}I_i^{\mu,\Xi^*K}, \tag{A28}$$

$$\Gamma_i^\mu(\Sigma^0) = \frac{\mathcal{C}^2((c_1+3c_2+3)Q^2+12m_\Delta^2)}{9f^2(4m_\Delta^2+Q^2)}I_i^{\mu,\Delta K}$$
$$-\frac{\mathcal{C}^2((c_1+3c_2+3)Q^2+12m_{\Xi^*}^2)}{36f^2(4m_{\Xi^*}^2+Q^2)}I_i^{\mu,\Xi^*K}, \tag{A29}$$

$$\Gamma_i^\mu(\Sigma^+) = \frac{\mathcal{C}^2((c_1+3c_2+3)Q^2+12m_{\Sigma^*}^2)}{36f^2(4m_{\Sigma^*}^2+Q^2)}I_i^{\mu,\Sigma^*\pi}$$
$$+\frac{7\mathcal{C}^2((c_1+3c_2+3)Q^2+12m_\Delta^2)}{18f^2(4m_\Delta^2+Q^2)}I_i^{\mu,\Delta K}, \tag{A30}$$

where the integral $I_i^{\mu,TM}$ is written as

$$I_i^{\mu,TM} = \bar{u}(p')\tilde{F}(q)\int\frac{d^4k}{(2\pi)^4}\frac{\tilde{F}(k)^2}{D_M(k)}(k^\sigma+z\not{k}\gamma^\sigma) \tag{A31}$$

$$\times\frac{1}{\not{p}'-\not{k}-m_T}S_{\sigma\alpha}(p'-k)\gamma^{\alpha\beta\mu}\frac{1}{\not{p}-\not{k}-m_T}$$
$$\times S_{\beta\rho}(p-k)(k^\rho+z\gamma^\rho\not{k})u(p). \tag{A32}$$

The contribution for Fig. 1(j) is written as

$$\Gamma_j^\mu(\Sigma^-) = \frac{(c_1+3c_2)\mathcal{C}^2 m_{\Sigma^*}}{18f^2(4m_{\Sigma^*}^2+Q^2)}I_j^{\mu,\Sigma^*\pi}+\frac{(c_1+3c_2)\mathcal{C}^2 m_\Delta}{3f^2(4m_\Delta^2+Q^2)}I_j^{\mu,\Delta K}$$
$$+\frac{(c_1+3c_2)\mathcal{C}^2 m_{\Xi^*}}{9f^2(4m_{\Xi^*}^2+Q^2)}I_j^{\mu,\Xi^*K}, \tag{A33}$$

$$\Gamma_j^\mu(\Sigma^0) = -\frac{2(c_1+3c_2)\mathcal{C}^2 m_\Delta}{9f^2(4m_\Delta^2+Q^2)}I_j^{\mu,\Delta K}$$
$$+\frac{(c_1+3c_2)\mathcal{C}^2 m_{\Xi^*}}{18f^2(4m_{\Xi^*}^2+Q^2)}I_j^{\mu,\Xi^*K}, \tag{A34}$$

$$\Gamma_j^\mu(\Sigma^+) = -\frac{(c_1+3c_2)\mathcal{C}^2 m_{\Sigma^*}}{18f^2(4m_{\Sigma^*}^2+Q^2)}I_j^{\mu,\Sigma^*\pi}$$
$$-\frac{7(c_1+3c_2)\mathcal{C}^2 m_\Delta}{9f^2(4m_\Delta^2+Q^2)}I_j^{\mu,\Delta K}, \tag{A35}$$

where the integral $I_j^{\mu,TM}$ is expressed as

$$I_j^{\mu,TM} = \bar{u}(p')\tilde{F}(q)\int\frac{d^4k}{(2\pi)^4}\frac{\tilde{F}(k)^2}{D_M(k)}(k^\sigma+z\not{k}\gamma^\sigma) \tag{A36}$$

$$\times\frac{1}{\not{p}'-\not{k}-m_T}S_{\sigma\nu}(p'-k)i\sigma^{\mu\lambda}q_\lambda\frac{1}{\not{p}-\not{k}-m_T}$$
$$\times S^{\nu\rho}(p-k)(k_\rho+z\gamma_\rho\not{k})u(p). \tag{A37}$$

The contribution for the intermediate octet-decuplet transition diagrams Figs. 1(k) and 1(l) is expressed as

$$\Gamma^{\mu}_{k+l}(\Sigma^-) = -\frac{c_1 \mathcal{C}F}{12f^2 m_\Sigma} I^{\mu,\Sigma^*\Sigma\pi}_{k+l} + \frac{c_1 \mathcal{C}D}{12f^2 m_\Lambda} I^{\mu,\Sigma^*\Lambda\pi}_{k+l} + \frac{c_1 \mathcal{C}(D-F)}{6f^2 m_N} I^{\mu,\Delta NK}_{k+l},$$

(A38)

$$\Gamma^{\mu}_{k+l}(\Sigma^0) = -\frac{c_1 \mathcal{C}F}{6f^2 m_\Sigma} I^{\mu,\Sigma^*\Sigma\pi}_{k+l} - \frac{c_1 \mathcal{C}(D+F)}{12f^2 m_\Xi} I^{\mu,\Xi^*\Xi K}_{k+l},$$

(A39)

$$\Gamma^{\mu}_{k+l}(\Sigma^+) = -\frac{c_1 \mathcal{C}F}{4f^2 m_\Sigma} I^{\mu,\Sigma^*\Sigma\pi}_{k+l} - \frac{c_1 \mathcal{C}D}{12f^2 m_\Lambda} I^{\mu,\Sigma^*\Lambda\pi}_{k+l} - \frac{c_1 \mathcal{C}(D-F)}{6f^2 m_N} I^{\mu,\Delta NK}_{k+l} - \frac{c_1 \mathcal{C}(D+F)}{6f^2 m_\Xi} I^{\mu,\Xi^*\Xi K}_{k+l},$$

(A40)

where the integral $I^{\mu,TBM}_{k+l}$ is written as

$$
\begin{aligned}
I^{\mu,TBM}_{k+l} = \bar{u}(p')\tilde{F}(q) \int \frac{\mathrm{d}^4 k}{(2\pi)^4} \frac{\tilde{F}(k)^2}{D_M(k)} & \left\{ \slashed{k}\gamma_5 \frac{1}{\slashed{p}' - \slashed{k} - m_B}(-\slashed{q})\gamma_5 \frac{1}{\slashed{p} - \slashed{k} - m_T} S^{\mu\rho}(p-k)(k_\rho + z\gamma_\rho \slashed{k}) \right. \\
& + \slashed{k}\gamma_5 \frac{1}{\slashed{p}' - \slashed{k} - m_B}\gamma^\mu\gamma_5 q_\nu \frac{1}{\slashed{p} - \slashed{k} - m_T} S^{\nu\rho}(p-k)(k_\rho + z\gamma_\rho \slashed{k}) \\
& + (k_\nu + z\slashed{k}\gamma_\nu) \frac{1}{\slashed{p}' - \slashed{k} - m_T} S^{\nu\rho}(p'-k)(-q_\rho)\gamma^\mu\gamma_5 \frac{1}{\slashed{p} - \slashed{k} - m_B} \slashed{k}\gamma_5 \\
& \left. + (k_\nu + z\slashed{k}\gamma_\nu) \frac{1}{\slashed{p}' - \slashed{k} - m_T} S^{\nu\mu}(p'-k)\slashed{q}\gamma_5 \frac{1}{\slashed{p} - \slashed{k} - m_B} \slashed{k}\gamma_5 \right\} u(p).
\end{aligned}
$$

(A41)

The contribution for the Kroll-Ruderman diagrams Figs. 1(m) and 1(n) is written as

$$\Gamma^{\mu}_{m+n}(\Sigma^-) = \frac{\mathcal{C}^2}{12f^2} I^{\mu,\Sigma^*\pi}_{m+n} + \frac{\mathcal{C}^2}{6f^2} I^{\mu,\Delta K}_{m+n},$$

(A42)

$$\Gamma^{\mu}_{m+n}(\Sigma^0) = \frac{\mathcal{C}^2}{3f^2} I^{\mu,\Delta K}_{m+n} - \frac{\mathcal{C}^2}{12f^2} I^{\mu,\Sigma^*K}_{m+n},$$

(A43)

$$\Gamma^{\mu}_{m+n}(\Sigma^+) = -\frac{\mathcal{C}^2}{12f^2} I^{\mu,\Sigma^*\pi}_{m+n} + \frac{\mathcal{C}^2}{2f^2} I^{\mu,\Delta K}_{m+n} - \frac{\mathcal{C}^2}{6f^2} I^{\mu,\Xi^*K}_{m+n},$$

(A44)

where the integral $I^{\mu,TM}_{m+n}$ is written as

$$
\begin{aligned}
I^{\mu,TM}_{m+n} = \bar{u}(p')\tilde{F}(q) \int \frac{\mathrm{d}^4 k}{(2\pi)^4} \frac{\tilde{F}(k)^2}{D_M(k)} & \left\{ (k_\sigma + z\slashed{k}\gamma_\sigma) \frac{1}{\slashed{p}' - \slashed{k} - m_T} S^{\sigma\rho}(p'-k)(g^{~\mu}_{\rho} + z\gamma_\rho \gamma^\mu) \right. \\
& \left. + (g^{\mu}_{~\sigma} + z\gamma^\mu\gamma_\sigma) \frac{1}{\slashed{p} - \slashed{k} - m_T} S^{\sigma\rho}(p-k)(k_\rho + z\gamma_\rho \slashed{k}) \right\} u(p).
\end{aligned}
$$

(A45)

The contribution for the additional diagrams with intermediate decuplet states Figs. 1(o) and 1(p) is expressed as

$$\Gamma^{\mu}_{o+p}(\Sigma^-) = \frac{\mathcal{C}^2}{12f^2} I^{\mu,\Sigma^*\pi}_{o+p} + \frac{\mathcal{C}^2}{6f^2} I^{\mu,\Delta K}_{o+p},$$

(A46)

$$\Gamma^{\mu}_{o+p}(\Sigma^0) = \frac{\mathcal{C}^2}{3f^2} I^{\mu,\Delta K}_{o+p} - \frac{\mathcal{C}^2}{12f^2} I^{\mu,\Sigma^*K}_{o+p},$$

(A47)

$$\Gamma^{\mu}_{o+p}(\Sigma^+) = -\frac{\mathcal{C}^2}{12f^2} I^{\mu,\Sigma^*\pi}_{o+p} + \frac{\mathcal{C}^2}{2f^2} I^{\mu,\Delta K}_{o+p} - \frac{\mathcal{C}^2}{6f^2} I^{\mu,\Xi^*K}_{o+p},$$

(A48)

where the integral $I^{\mu,TM}_{o+p}$ is written as

$$I_{o+p}^{\mu,TM} = \bar{u}(p')\tilde{F}(q) \int \frac{d^4k}{(2\pi)^4} \frac{\tilde{F}(k)}{D_M(k)}$$

$$\times \left\{ \frac{(-2k+q)^\mu}{-2kq+q^2} (\tilde{F}(k-q) - \tilde{F}(k))(k_\sigma + z\slashed{k}\gamma_\sigma) \frac{1}{\slashed{p}' - \slashed{k} - m_T} S^{\sigma\rho}(p'-k)((k-q)_\rho + z\gamma_\rho(\slashed{k} - \slashed{q})) \right.$$

$$\left. + \frac{(2k+q)^\mu}{2kq+q^2} (\tilde{F}(k+q) - \tilde{F}(k))((k+q)_\sigma + z(\slashed{k} + \slashed{q})\gamma_\sigma) \frac{1}{\slashed{p} - \slashed{k} - m_T} S^{\sigma\rho}(p-k)(k_\rho + z\gamma_\rho\slashed{k}) \right\} u(p). \quad \text{(A49)}$$

Using Package-X [74] to simplify the loop integral, we can get the results for the Dirac and Pauli form factors.

---

[1] A. Camsonne *et al.* (Jefferson Lab Hall A Collaboration), JLab Measurement of the ^{4}He Charge Form Factor at Large Momentum Transfers, Phys. Rev. Lett. **112**, 132503 (2014).

[2] A. M. Sirunyan *et al.* (CMS Collaboration), Measurement of the triple-differential dijet cross section in proton-proton collisions at $\sqrt{s} = 8$ TeV and constraints on parton distribution functions, Eur. Phys. J. C **77**, 746 (2017).

[3] W. Xiong *et al.*, A small proton charge radius from an electron–proton scattering experiment, Nature (London) **575**, 147 (2019).

[4] J. Bernauer *et al.* (A1 Collaboration), High-Precision Determination of the Electric and Magnetic Form Factors of the Proton, Phys. Rev. Lett. **105**, 242001 (2010).

[5] K. Kubodera, Y. Kohyama, K. Oikawa, and C. W. Kim, Weak-interaction form factors of octet baryons in the cloudy bag model, Nucl. Phys. **A439**, 695 (1985).

[6] H. Dahiya, N. Sharma, P. K. Chatley, and G. Manmoha, Semileptonic octet baryon weak axial-vector form factors in the chiral constituent quark model, AIP Conf. Proc. **1149**, 361 (2009).

[7] J.-Y. Kim and H.-C. Kim, Electromagnetic form factors of singly heavy baryons in the self-consistent SU(3) chiral quark-soliton model, Phys. Rev. D **97**, 114009 (2018).

[8] T. Ito, W. Bentz, I. Cloët, A. Thomas, and K. Yazaki, The NJL-jet model for quark fragmentation functions, Phys. Rev. D **80**, 074008 (2009).

[9] T. Ohlsson and H. Snellman, Weak form factors for semileptonic octet baryon decays in the chiral quark model, Eur. Phys. J. C **6**, 285 (1999).

[10] Y. Yang, D.-Y. Chen, and Z. Lu, The electromagnetic form factors of Λ hyperon in the vector meson dominance model, Phys. Rev. D **100**, 073007 (2019).

[11] C. S. An and B. Saghai, Strangeness magnetic form factor of the proton in the extended chiral quark model, Phys. Rev. C **88**, 025206 (2013).

[12] R. N. Faustov and V. O. Galkin, Relativistic description of the Ξ_b baryon semileptonic decays, Phys. Rev. D **98**, 093006 (2018).

[13] T. Fuchs, J. Gegelia, and S. Scherer, Electromagnetic form factors of the nucleon in chiral perturbation theory, J. Phys. G **30**, 1407 (2004).

[14] B. Kubis and U.-G. Meissner, Low-energy analysis of the nucleon electromagnetic form factors, Nucl. Phys. **A679**, 698 (2001).

[15] P. Wang, D. B. Leinweber, A. W. Thomas, and R. D. Young, Chiral extrapolation of nucleon magnetic form factors, Phys. Rev. D **75**, 073012 (2007).

[16] P. Wang, D. B. Leinweber, A. W. Thomas, and R. D. Young, Strange magnetic form factor of the proton at $Q^2 = 0.23$ GeV^2, Phys. Rev. C **79**, 065202 (2009).

[17] P. Wang, D. B. Leinweber, A. W. Thomas, and R. D. Young, Chiral extrapolation of nucleon magnetic moments at next-to-leading order, Phys. Rev. D **86**, 094038 (2012).

[18] J. M. M. Hall, D. B. Leinweber, and R. Young, Finite-volume and partial quenching effects in the magnetic polarizability of the neutron, Phys. Rev. D **89**, 054511 (2014).

[19] P. Wang, D. B. Leinweber, and A. W. Thomas, Strange magnetic form factor of the nucleon in a chiral effective model at next-to-leading order, Phys. Rev. D **89**, 033008 (2014).

[20] P. Wang, D. B. Leinweber, and A. W. Thomas, Pure sea-quark contributions to the magnetic form factors of Σ baryons, Phys. Rev. D **92**, 034508 (2015).

[21] H. Li, P. Wang, D. B. Leinweber, and A. W. Thomas, Spin of the proton in chiral effective field theory, Phys. Rev. C **93**, 045203 (2016).

[22] H. Li and P. Wang, Chiral extrapolation of nucleon axial charge ga in effective field theory, Chin. Phys. C **40**, 123106 (2016).

[23] C. R. Allton, W. Armour, D. B. Leinweber, A. W. Thomas, and R. D. Young, Chiral and continuum extrapolation of partially-quenched lattice results, Phys. Lett. B **628**, 125 (2005).

[24] P. Wang, D. Leinweber, A. Thomas, and R. Young, Chiral extrapolation of octet-baryon charge radii, Phys. Rev. D **79**, 094001 (2009).

[25] F. He and P. Wang, Nucleon electromagnetic form factors with a nonlocal chiral effective Lagrangian, Phys. Rev. D **97**, 036007 (2018).

[26] F. He and P. Wang, Strange form factors of the nucleon with a nonlocal chiral effective Lagrangian, Phys. Rev. D **98**, 036007 (2018).

[27] Y. Salamu, C.-R. Ji, W. Melnitchouk, A. W. Thomas, and P. Wang, Parton distributions from nonlocal chiral SU(3) effective theory: Splitting functions, Phys. Rev. D **99**, 014041 (2019).

[28] F. He and P. Wang, Sivers distribution functions of sea quark in proton with chiral Lagrangian, Phys. Rev. D **100,** 074032 (2019).

[29] F. He and P. Wang, Pauli form factors of electron and muon in nonlocal quantum electrodynamics, Eur. Phys. J. Plus **135,** 156 (2020).

[30] S. Boinepalli, D. Leinweber, A. Williams, J. Zanotti, and J. Zhang, Precision electromagnetic structure of octet baryons in the chiral regime, Phys. Rev. D **74,** 093005 (2006).

[31] P. Shanahan, A. Thomas, R. Young, J. Zanotti, R. Horsley, Y. Nakamura, D. Pleiter, P. Rakow, G. Schierholz, and H. Stüben (CSSM and QCDSF/UKQCD Collaborations), Magnetic form factors of the octet baryons from lattice QCD and chiral extrapolation, Phys. Rev. D **89,** 074511 (2014).

[32] P. Shanahan, A. Thomas, R. Young, J. Zanotti, R. Horsley, Y. Nakamura, D. Pleiter, P. Rakow, G. Schierholz, and H. Stüben, Electric form factors of the octet baryons from lattice QCD and chiral extrapolation, Phys. Rev. D **90,** 034502 (2014).

[33] B. Kubis and U. G. Meissner, Baryon form-factors in chiral perturbation theory, Eur. Phys. J. C **18,** 747 (2001).

[34] Y. Xiao, X.-L. Ren, J.-X. Lu, L.-S. Geng, and U.-G. Meiner, Octet baryon magnetic moments at next-to-next-to-leading order in covariant chiral perturbation theory, Eur. Phys. J. C **78,** 489 (2018).

[35] L. Geng, J. M. Camalich, and M. V. Vacas, Leading-order decuplet contributions to the baryon magnetic moments in chiral perturbation theory, Phys. Lett. B **676,** 63 (2009).

[36] A. H. Blin, Systematic study of octet-baryon electromagnetic form factors in covariant chiral perturbation theory, Phys. Rev. D **96,** 093008 (2017).

[37] E. E. Jenkins, Baryon masses in chiral perturbation theory, Nucl. Phys. **B368,** 190 (1992).

[38] E. E. Jenkins, M. E. Luke, A. V. Manohar, and M. J. Savage, Chiral perturbation theory analysis of the baryon magnetic moments, Phys. Lett. B **302,** 482 (1993); Erratum, Phys. Lett. B **388,** 866 (1996).

[39] P. Wang, Solid quantization for nonpoint particles, Can. J. Phys. **92,** 25 (2014).

[40] B. Borasoy and U.-G. Meissner, Chiral expansion of baryon masses and σ-terms, Ann. Phys. (N.Y.) **254,** 192 (1997).

[41] M. Luty and M. J. White, Decouplet contributions to hyperon axial vector form factors, Phys. Lett. B **319,** 261 (1993).

[42] L. M. Nath, B. Etemadi, and J. D. Kimel, Uniqueness of the interaction involving spin-$\frac{3}{2}$ particles, Phys. Rev. D **3,** 2153 (1971).

[43] M. E. Carrillo-Serrano, W. Bentz, I. C. Cloët, and A. W. Thomas, Baryon octet electromagnetic form factors in a confining NJL model, Phys. Lett. B **759,** 178 (2016).

[44] X. Liu, K. Khosonthongkee, A. Limphirat, and Y. Yan, Study of baryon octet electromagnetic form factors in perturbative chiral quark model, J. Phys. G **41,** 055008 (2014).

[45] H.-W. Lin and K. Orginos, Strange baryon electromagnetic form factors and SU(3) flavor symmetry breaking, Phys. Rev. D **79,** 074507 (2009).

[46] M. Tanabashi *et al.* (Particle Data Group), Review of particle physics, Phys. Rev. D **98,** 030001 (2018).

[47] T. Bauer, J. Bernauer, and S. Scherer, Electromagnetic form factors of the nucleon in effective field theory, Phys. Rev. C **86,** 065206 (2012).

[48] T. Janssens, R. Hofstadter, E. Hughes, and M. Yearian, Proton form factors from elastic electron-proton scattering, Phys. Rev. **142,** 922 (1966).

[49] C. Berger, V. Burkert, G. Knop, B. Langenbeck, and K. Rith, Electromagnetic form-factors of the proton at squared four momentum transfers between 10 and 50 fm^{-2}, Phys. Lett. B **35,** 87 (1971).

[50] L. Price, J. Dunning, M. Goitein, K. Hanson, T. Kirk, and R. Wilson, Backward-angle electron-proton elastic scattering and proton electromagnetic form-factors, Phys. Rev. D **4,** 45 (1971).

[51] H. Anklin *et al.*, Precision measurement of the neutron magnetic form factor, Phys. Lett. B **336,** 313 (1994).

[52] R. Walker *et al.*, Measurements of the proton elastic form-factors for $1 \leq Q^2 \leq 3 (\text{GeV}/C)^2$ at SLAC, Phys. Rev. D **49,** 5671 (1994).

[53] W. Bartel, F. Busser, W. Dix, R. Felst, D. Harms, H. Krehbiel, P. Kuhlmann, J. McElroy, J. Meyer, and G. Weber, Measurement of proton and neutron electromagnetic form-factors at squared four momentum transfers up to 3-GeV/c^2, Nucl. Phys. **B58,** 429 (1973).

[54] K. Hanson, J. Dunning, M. Goitein, T. Kirk, L. Price, and R. Wilson, Large angle quasielastic electron-deuteron scattering, Phys. Rev. D **8,** 753 (1973).

[55] J. Arrington, W. Melnitchouk, and J. A. Tjon, Global analysis of proton elastic form factor data with two-photon exchange corrections, Phys. Rev. C **76,** 035205 (2007).

[56] J. Golak, G. Ziemer, H. Kamada, H. Witala, and W. Gloeckle, Extraction of electromagnetic neutron form-factors through inclusive and exclusive polarized electron scattering on polarized ^3He target, Phys. Rev. C **63,** 034006 (2001).

[57] P. Markowitz *et al.*, Measurement of the magnetic form factor of the neutron, Phys. Rev. C **48,** R5 (1993).

[58] E. Bruins *et al.*, Measurement of the Neutron Magnetic Form Factor, Phys. Rev. Lett. **75,** 21 (1995).

[59] H. Anklin *et al.*, Precise measurements of the neutron magnetic form factor, Phys. Lett. B **428,** 248 (1998).

[60] W. Xu *et al.*, Transverse Asymmetry $A_{T'}$ from Quasielastic Polarized $^3\vec{\text{He}}(\vec{e}, e')$ Process and the Neutron Magnetic Form Factor, Phys. Rev. Lett. **85,** 2900 (2000).

[61] G. Kubon *et al.*, Precise neutron magnetic form-factors, Phys. Lett. B **524,** 26 (2002).

[62] R. Madey *et al.* (E93-038 Collaboration), Measurements of G_E^n/G_M^n from the $^2\text{H}(\vec{e}, e'\vec{n})^1\text{H}$ Reaction to $Q^2 = 1.45 \ (\text{GeV}/c)^2$, Phys. Rev. Lett. **91,** 122002 (2003).

[63] W. Xu *et al.* (Jefferson Lab E95-001 Collaboration), Plane-wave impulse approximation extraction of the neutron magnetic form factor from quasielastic $^3\text{He} \rightarrow (\vec{e}, e')$ at $Q^2 = 0.3$ to 0.6, Phys. Rev. C **67,** 012201(R) (2003).

[64] J. Murphy, Y. Shin, and D. Skopik, Proton form factor from 0.15 to 0.79 fm^{-2}, Phys. Rev. C **9,** 2125 (1974); Erratum, Phys. Rev. C **10,** (1974).

[65] G. Hohler, E. Pietarinen, I. Sabba Stefanescu, F. Borkowski, G. Simon, V. Walther, and R. Wendling, Analysis of

electromagnetic nucleon form-factors, Nucl. Phys. **B114**, 505 (1976).

[66] G. Simon, C. Schmitt, F. Borkowski, and V. Walther, Absolute electron proton cross-sections at low momentum transfer measured with a high pressure gas target system, Nucl. Phys. **A333**, 381 (1980).

[67] T. Eden *et al.*, Electric form factor of the neutron from the ^{2}H$(\vec{e}e'\vec{n})^1$H reaction at $Q^2 = 0.255$ (GeV/c)^2, Phys. Rev. C **50**, R1749(R) (1994).

[68] C. Herberg *et al.*, Determination of the neutron electric form-factor in the D(e,e' n)p reaction and the influence of nuclear binding, Eur. Phys. J. A **5**, 131 (1999).

[69] M. Ostrick *et al.*, Measurement of the Neutron Electric Form Factor $G_{E,n}$ in the Quasifree ^{2}H$(\vec{e}, e'\vec{n})p$ Reaction, Phys. Rev. Lett. **83**, 276 (1999).

[70] I. Passchier *et al.*, Charge Form Factor of the Neutron from the Reaction $^2\vec{H}(\vec{e}, e'n)p$, Phys. Rev. Lett. **82**, 4988 (1999).

[71] J. Bermuth *et al.*, The neutron charge form-factor and target analyzing powers from polarized-$^3He(e \rightarrow, e)'n$ scattering, Phys. Lett. B **564**, 199 (2003).

[72] G. Warren *et al.* (Jefferson Lab E93-026 Collaboration), Measurement of the Electric Form Factor of the Neutron at $Q^2 = 0.5$ and 1.0 GeV^2/c^2, Phys. Rev. Lett. **92**, 042301 (2004).

[73] D. Glazier *et al.*, Measurement of the electric form factor of the neutron at $Q^2 = 0.3$–0.8 (GeV/c)^2, Eur. Phys. J. A **24**, 101 (2005).

[74] H. H. Patel, Package-X: A Mathematica package for the analytic calculation of one-loop integrals, Comput. Phys. Commun. **197**, 276 (2015).